PNAS RESEARCH ARTICLE | IMMUNOLOGY AND INFLAMMATION

The Maresin 1–LGR6 axis decreases respiratory syncytial virus-induced lung inflammation

Nandini Krishnamoorthy[a,1], Katherine H. Walker[a,2], Thayse R. Brüggemann[a,2], Luciana P. Tavares[a], Ethan W. Smith[a], Julie Nijmeh[a], Yan Bai[b], Xingbin Ai[b], R. Elaine Cagnina[a], Melody G. Duvall[a], Jessica A. Lehoczky[c], and Bruce D. Levy[a,1]

Edited by Harvey Cantor, Dana-Farber Cancer Institute, Boston, MA; received April 27, 2022; accepted November 29, 2022

The resolution of infection is an active process with specific molecular and cellular mechanisms that temper inflammation and enhance pathogen clearance. Here, the specialized pro-resolving mediator (SPM) Maresin 1 (MaR1) inhibited respiratory syncytial virus (RSV)-induced inflammation. inlerleukin-13 production from type 2 innate lymphoid cells (ILC) and CD4 T helper type 2 cells was decreased by exogenous MaR1. In addition, MaR1 increased amphiregulin production and decreased RSV viral transcripts to promote resolution. MaR1 also promoted interferon-β production in mouse lung tissues and also in pediatric lung slices. MaR1 significantly inhibited the RSV-triggered aberrant inflammatory phenotype in FoxP3-expressing Tregs. The receptor for MaR1, leucine-rich repeat-containing G protein-coupled receptor 6 (LGR6), was constitutively expressed on Tregs. Following RSV infection, mice lacking Lgr6 had exacerbated type 2 immune responses with an increased viral burden and blunted responses to MaR1. Together, these findings have uncovered a multi-pronged protective signaling axis for MaR1–Lgr6, improving Tregs's suppressive function and upregulating host antiviral genes resulting in decreased viral burden and pathogen-mediated inflammation, ultimately promoting restoration of airway mucosal homeostasis.

resolution of inflammation | specialized pro-resolving mediators | regulatory T cells | innate lymphoid cells | CD4 T helper type 2 cells

Significance

Respiratory syncytial virus (RSV) is a leading cause of severe viral bronchiolitis among children, the elderly, and immunocompromised patients. Unresolved and prolonged immune responses to RSV can lead to respiratory failure. Regulatory T cells (Tregs) work to subvert inflammation; however, RSV hijacks the Treg machinery to imprint a prophlogistic phenotype. Here, we have determined that the specialized pro-resolving mediator Maresin 1 (MaR1) signaling via its receptor Leucine-Rich Repeat-Containing G Protein-Coupled Receptor 6 (LGR6) can reverse the RSV-induced maladaptive Treg programming and decrease inflammation. These findings have uncovered a molecular counter-regulatory mechanism that limits pathogen-induced lung immunopathology and hastens the resolution of an important respiratory viral infection.

Respiratory syncytial virus (RSV) is a major cause of lower tract respiratory infections in children and is a leading cause of infant hospitalization in the United States (1). RSV infection is also seen in adults and is the second leading cause of death associated with viral infections in the elderly (2, 3). Chronic Obstructive Pulmonary Disorder (COPD) patients are also susceptible to RSV infection resulting in exacerbations (4, 5). RSV infection typically presents as a mild and self-resolving infection; however, in some children, particularly those less than 2 y old, an overexuberant immune response to the virus results in severe bronchiolitis and even respiratory failure evidenced pathologically by occlusion of the airways with cellular debris and mucus (6). Potential mechanisms to curtail the pathologic unwarranted airway inflammation and injury with RSV would provide needed therapeutic relief for vulnerable patients.

Regulatory T cells (Tregs) express the canonical transcription factor FoxP3 and subvert inflammation to maintain immunological homeostasis (7). RSV infection disables Tregs and programs them to become prophlogistic cells (8). These RSV Tregs retain FoxP3-expression but also express the type 2 associated cytokine inlerleukin-13 (IL-13) and transcription factor GATA-3 that exacerbate virus-induced immunopathology. Broadly, the acquisition of a prophlogistic phenotype by Tregs is linked to the pathophysiology of several common inflammatory diseases. Mechanisms to restore these pathologic Tregs to their protective phenotype and suppressive function under inflammatory conditions remain to be determined.

Counter-regulatory cell mechanisms are generally responsive to environmental cues. The resolution of inflammation is mediated in part by specialized pro-resolving mediators (SPMs), a family of endogenous molecules that can limit pathogen-induced inflammation and accelerate pathogen clearance (9, 10). These mediators are produced from essential fatty acids during tissue inflammation and carry potent anti-inflammatory and pro-resolving functions (11). SPMs can exert cell-specific actions via their receptors and deficiency in receptor expression in mouse and human studies correlate with delayed resolution (9). Dietary docosahexaenoic acid (DHA) supplementation during pregnancy in mothers with lower endogenous levels of this omega-3 fatty acid can lead to a lower risk of wheezing and respiratory infections in infants, highlighting the potential immunoregulatory effects of essential omega-3 fatty acid-derived mediators in human health (12).

Here, in a self-limited mouse model of RSV infection, the administration of the DHA-derived SPM Maresin 1 (MaR1; 7R,14S-dihydroxy-docosa-4Z,8E,10E,12Z,16Z,19Z-hexaenoic acid)

Competing interest statement: The authors declare competing interest. The authors have patent filings to disclose. B.D.L. is an inventor on patents (resolvins) assigned to Brigham and Women's Hospital (BWH). His interests were reviewed and are managed by the BWH according to conflict of interest policies. The other authors have no conflicts of interest to declare.

This article is a PNAS Direct Submission.

[1]To whom correspondence may be addressed. Email: nkrishnamoorthy@bwh.harvard.edu or blevy@bwh.harvard.edu.

[2]K.H.W. and T.R.B. contributed equally to this work.

This article contains supporting information online at https://www.pnas.org/lookup/suppl/doi:10.1073/pnas.2206480120/-/DCSupplemental.

Published January 3, 2023.

decreased pulmonary inflammation and enhanced viral clearance. MaR1 reduced IL-13 production from type 2 innate lymphoid cells (ILC2s) and CD4 T helper type 2 (CD4 TH2) cells and increased lung amphiregulin (AREG) levels. MaR1's protective actions were mediated by Leucine-Rich Repeat-Containing G Protein Coupled Receptor 6 (LGR6) signaling with a prominent effector role for Tregs. These mechanistic findings translated to a model of ex vivo RSV infection of precision cut human pediatric lung slices. Taken together, these data have uncovered multipronged actions for MaR1 signaling via LGR6 to accelerate the resolution of inflammation in mouse and human experimental models of RSV infection.

Results

Maresin 1 Enhances Viral Clearance and Decreases Type 2 Inflammation after RSV Infection. To determine whether MaR1 could decrease the pathogen-evoked immune responses triggered by RSV and accelerate resolution, we first defined the inflammatory and resolution time course for mouse infection with a human clinical strain RSV line 19 (10^5 PFU) that is known to trigger IL-13 and mucous production (13). The pathologic consequences of infection of 3-wk-old mice were analyzed by histology and flow cytometry (*SI Appendix*, Fig. S1 *A* and *B*). On day 3 post-infection (pi), there were significant increases in IL-13 levels and viral titers (*SI Appendix*, Fig. S1 *C* and *D*). With increasing viral replication and inflammatory responses, this time point (Day 3) was chosen to administer MaR1 [10 ng; intranasal route (i.n.)] (Fig. 1*A*). This dose of MaR1 was chosen based on prior publications wherein exogenous administration of MaR1 in preclinical models of inflammation promoted resolution (14, 15). At day 6 pi, animals that received MaR1 had significantly decreased airway epithelial mucous cell metaplasia and reduced leukocyte infiltrates around the airways as determined by histopathological examination after Periodic Acid–Schiff (PAS) staining (Fig. 1*B*). We also looked at lung inflammation by H&E staining and found a significant increase in cellular infiltrate around the airways following RSV infection which was reduced with MaR1 administration (*SI Appendix*, Fig. S2 *A* and *B*). Given the role of Gob5 in driving mucus production, we analyzed mouse lungs following MaR1 administration. MaR1-treated mice had lower levels of *gob5* gene expression compared to the vehicle group (Fig. 1*C*). With the RSV-induced mucous cell metaplasia, IL-13 production from ILC2 ($IL13^+$ $Lineage^-$) and CD4 TH2 ($CD4^+IL\text{-}13^+$) cells peaked at day 6 pi (*SI Appendix*, Fig. S3). Compared with vehicle control, at day 6 pi, MaR1 administration significantly lowered IL-13 tissue levels (Fig. 1*D*) and decreased IL-13 production by ILC2 and CD4 TH2 cells (Fig. 1*E*).

Since MaR1 inhibited RSV-induced type 2 immune responses, we next evaluated whether it also promoted resolution of inflammation. MaR1 significantly increased levels of AREG in lung tissue compared to vehicle control at day 6 pi (Fig. 1*F*). Of note, RSV-infected lungs had barely detectable levels of this cytokine at this time point. In addition, MaR1 decreased RSV polymerase *L* gene expression at day 6 pi indicative of decreased amounts of actively replicating virus (Fig. 1*G*).

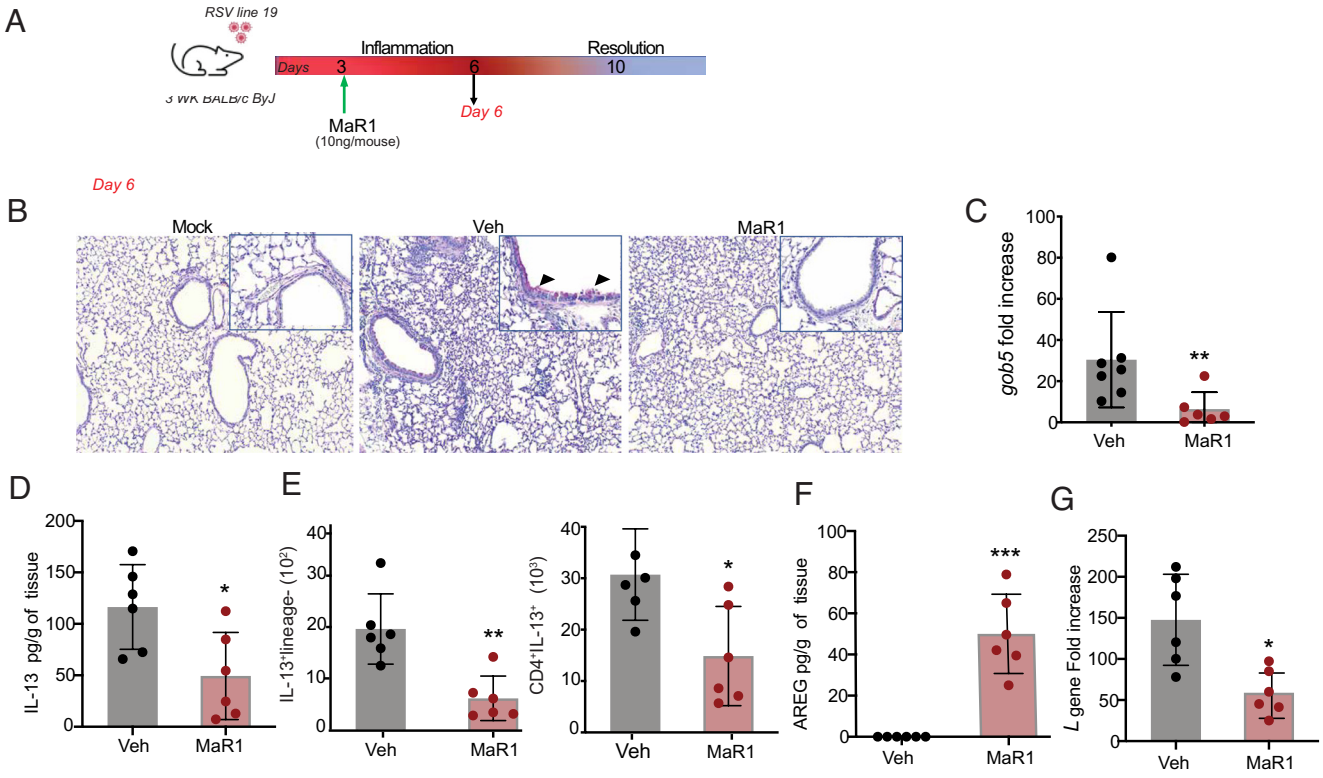

Fig. 1. Maresin 1 enhances viral clearance and decreases type 2 inflammation after RSV infection. (*A*) Schema of the mouse model of RSV infection with clinical strain *RSV line 19* (10^5 PFU/mouse, intranasal route, i.n.) in 3-wk old Balb/c ByJ mice. Vehicle or MaR1 (10 ng/mouse) administered i.n. on day 3 pi. Inflammatory and virological parameters analyzed on day 6 pi. (*B*) Representative lung tissue sections from mice 6 d post-mock infection (mock) or RSV infection with either i.n. vehicle (Veh) or MaR1 administered on day 3 pi (MaR1). Sections were stained with PAS. Original magnification (×10). *Inset* magnification (×20). Arrows indicate areas of high mucous production. (*C*) *gob5* expression analysis by qRT-PCR. Fold increase was calculated over mock infected mice. (*D*) IL-13 levels in lung tissue measured by Enzyme-linked immunosorbent assay (ELISA). (*E*) Number of $IL\text{-}13^+$ $Lineage^-$ ILC2 and $IL\text{-}13^+$ $CD4^+$ TH2 cells in the lungs with or without MaR1 exposure after RSV as measured by flow cytometry. (*F*) AREG levels in lung tissue with or without MaR1 exposure after RSV as measured by ELISA. (*G*) RSV *L* Gene expression analysis by qRT-PCR. Fold increase was calculated over mock infected mice. Values represent the mean ± SD. $^*P < 0.05$, $^{**}P < 0.01$, $^{***}P < 0.001$ and data were analyzed using Student's *t* test for all the panels shown here. This experiment was performed more than twice and the results from two experiments pooled. Each experiment used 3 to 4 mice per group.

Maresin 1 Promotes Resolution of RSV Infection with Increased AREG Production and Decreased Type 2 Inflammation. To determine whether the actions of MaR1 were transient, inflammatory responses at day 10 pi were next analyzed in the RSV mouse model (Fig. 2*A*). PAS staining of lung sections at day 10 pi revealed lower levels of mucous cell metaplasia compared to day 6 pi. Even with waning airway inflammation day 10 pi, relative to vehicle control, MaR1-exposed mice had less mucous cell metaplasia and cellular infiltrates (Fig. 2*B*). *gob5* gene transcripts showed decreased expression with MaR1 (Fig. 2*C*). Tissue levels of IL-13 decreased from day 6 to day 10 pi, and they were further lowered with MaR1 (Fig. 2*D*). ILC2 and CD4 TH2 cells were also decreased with MaR1 compared to vehicle at day 10 pi (Fig. 2*E*). AREG levels continued to show significantly increased levels at day 10 pi with MaR1 (Fig. 2*F*), and RSV *L* gene expression was further reduced on day 10 pi with MaR1 compared to vehicle (Fig. 2*G*). Taken together, these data indicate that MaR1 promoted resolution as a potent regulator of RSV-triggered inflammatory responses and viral transcripts, and a selective inducer of tissue AREG.

Unique Anti-viral Lung Gene Transcripts and Increased Interferon-β Production Following MaR1 Administration. In human and mouse models of RSV infection, IL-13 and type 2 immune responses to RSV have strongly correlated with disease severity (16). The ability of MaR1 to blunt viral gene transcripts could potentially be linked to reduced IL-13 levels seen in the mice. To identify this unique gene signature, we isolated RNA from mouse lungs 24 h following MaR1 administration (day 4 pi) and on day 6 pi. There were several time-dependent changes in gene expression belonging to the Toll-like receptor (TLR)-signaling pathway, Nucleotide-binding oligomerization domain (NOD)-like receptor pathway, retinoic acid-inducible gene I (RIG-I)-like receptor signaling, and type I interferon signaling and response on both day 4 pi and day 6 pi following MaR1 treatment. Importantly, some of the genes associated with innate immune responses (e.g., *Aim2, CARD9*) that were upregulated on day 4 pi with MaR1 either returned to baseline or were downregulated by day 6 pi. Similarly, members of the mitogen-activated protein (MAP) kinase family were activated on day 4 pi but showed decreased expression on day 6 pi (Fig. 3*A*). As shown on the heat map, we found interferon-β expression to be upregulated with MaR1 expression on day 4 pi with RSV, and this expression was sustained also on day 6 pi with RSV (Fig. 3*A*). RSV in known to inhibit interferon-β making the host vulnerable to reinfection (17). To validate induction of interferon-β transcript levels by MaR1, mouse lung tissues from day 4 pi and day 6 pi were analyzed for protein levels. On day 4 pi, levels of interferon-β showed a small trend toward increased expression with MaR1 treatment (Fig. 3*B*), and levels were significantly upregulated on day 6 pi compared to control group (Fig. 3*C*). Importantly,

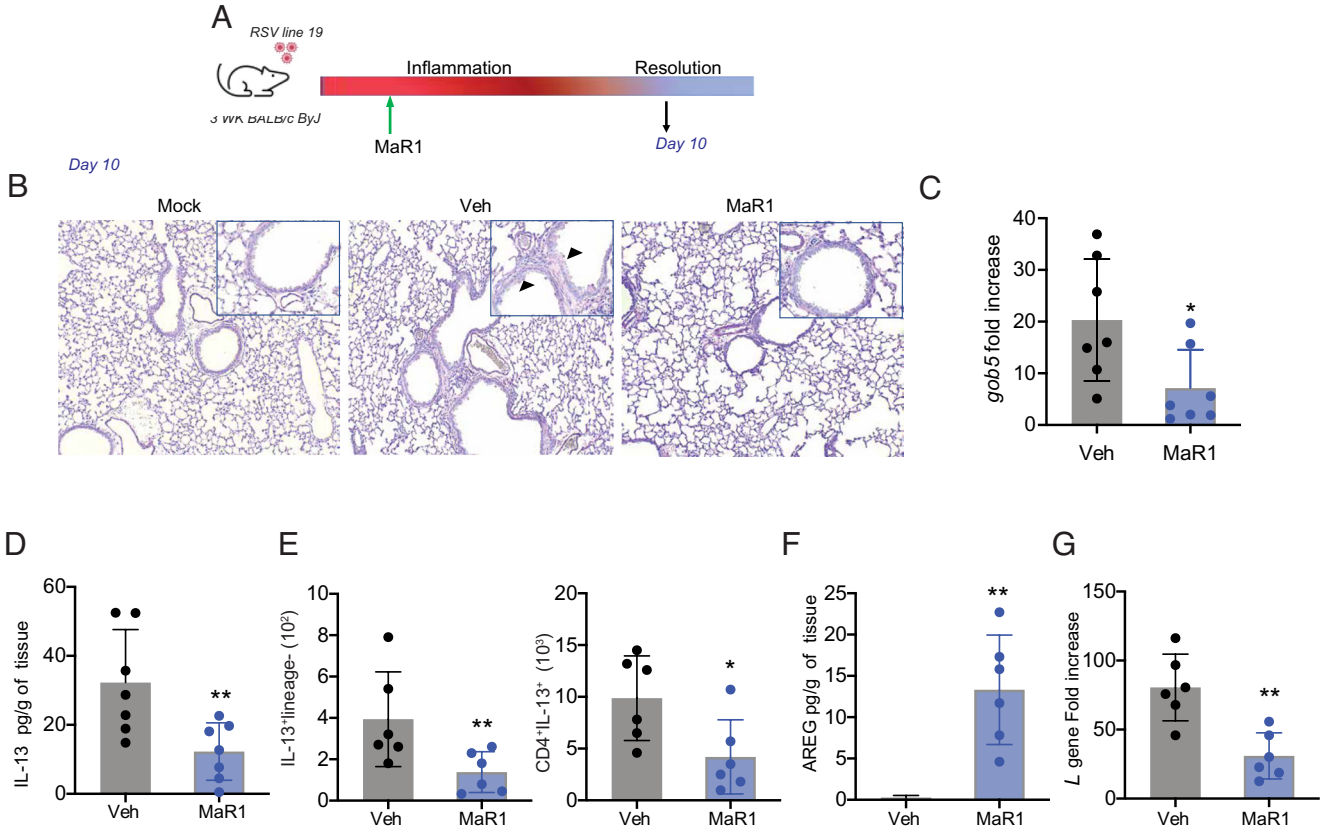

Fig. 2. Maresin 1 promotes resolution of RSV infection with increased AREG production and decreased type 2 inflammation. (*A*) Schema of the mouse model of RSV infection as in Fig. 1*A*. Inflammatory and virological parameters analyzed on day 10 pi. (*B*) Representative lung tissue sections from mice 10 d post-mock infection (mock) or RSV infection with either i.n. vehicle (Veh) or MaR1 administered on day 3 pi (MaR1). Sections were stained with PAS. Original magnification (×10). *Inset* magnification (×20). Arrows indicate areas of high mucous production. (*C*) *gob5* expression analysis by qRT-PCR Fold increase was calculated over mock infected mice. (*D*) IL-13 levels in lung tissue measured by ELISA. (*E*) Number of IL-13$^+$ Lineage$^-$ ILC2 and IL-13$^+$ CD4$^+$ TH2 cells in the lungs with or without MaR1 exposure after RSV as measured by flow cytometry. (*F*) AREG levels in lung tissue with or without MaR1 exposure after RSV as measured by ELISA. (*G*) RSV *L* gene expression analysis by qRT-PCR. Fold increase was calculated over mock infected mice. n≥3 mice per group. Values represent the mean ± SD. *$P < 0.05$, **$P < 0.01$, ***$P < 0.001$ and data were analyzed using Student's *t* test for all the panels shown here. This experiment was performed more than twice and the results from two experiments pooled. Each experiment used 3 to 4 mice per group.

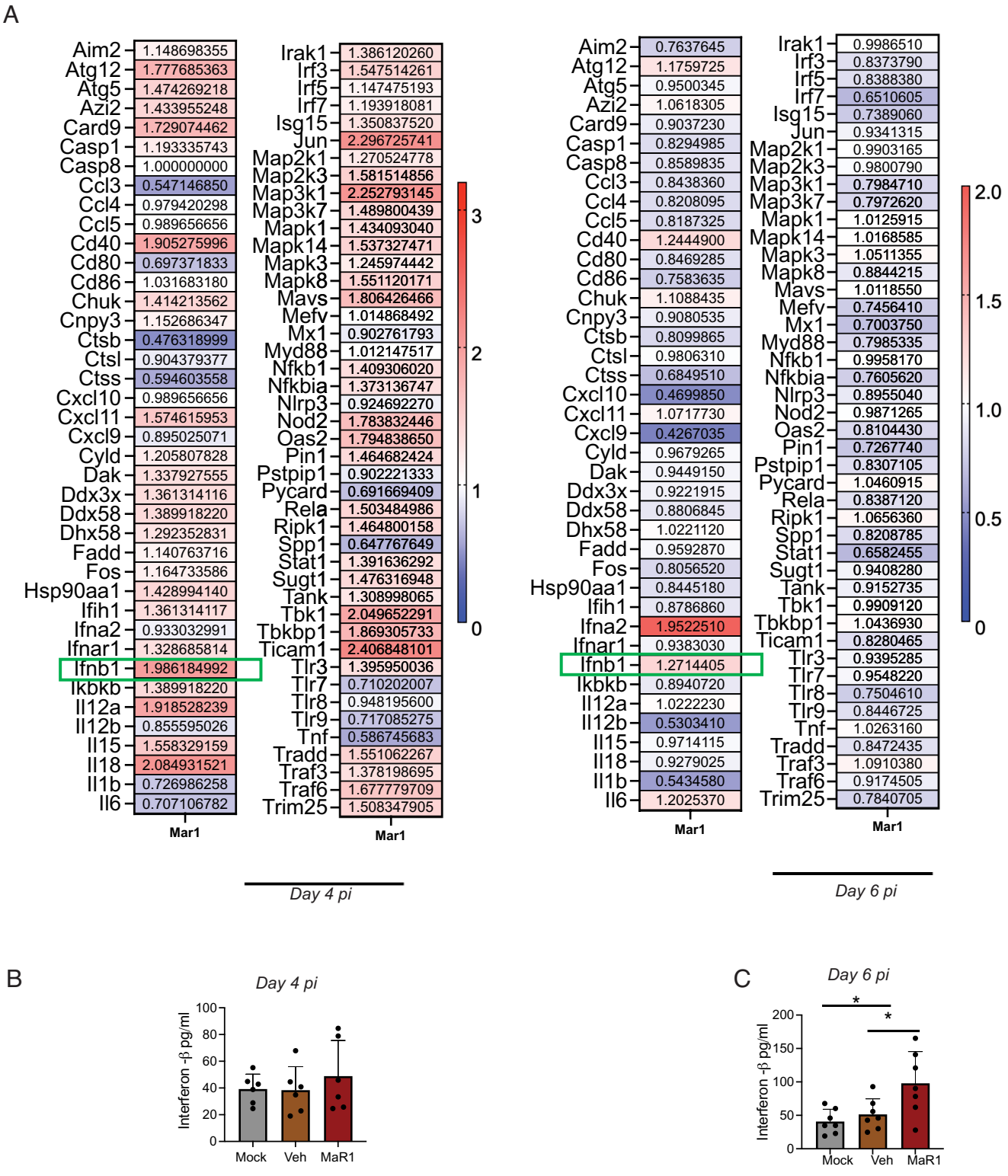

Fig. 3. Unique anti-viral lung gene transcripts and increased Interferon-β production following MaR1 administration. (*A*) Heat map showing fold change of gene transcripts in animals after MaR1 administration over Vehicle control. The gene expression was normalized to β-actin. The *Left* panel represents mice at day 4 pi and the *Right* panel represents mice at day 6 pi. For each time point 2 mice were used per group on two individual plates. The RNA was not pooled. The numbers in the heat map indicate the fold change of MaR-1-treated animals over Vehicle control. (*B*) Interferon-β concentration measured in ling tissue at day 4 pi as measured by legend plex ELISA. (*C*) Interferon-β concentration in ling tissue at day 6 pi as measured by legend plex ELISA. Values represent the mean ± SD and the data was analyzed using one-way ANOVA with Tukey's multiple comparisons test. *$P < 0.05$. For each group 3 to 4 mice were used per group per experiment. The experiments were performed twice.

RSV-infected lungs on day 4 pi and day 6 pi showed little change compared to the mock-infected group.

Alarmins and specific cytokines released from epithelial cells early in inflammation are known to trigger IL-13 production and activate type 2 immune response highlighting a potential role for MaR1 in inhibiting early cytokine release and thereby reducing overall type 2 response (18). Toward this goal, we analyzed mouse lung tissue at day 4 pi for levels of cytokines IL-33, TSLP, and

IL-25, all of which have been shown to play a critical role in modulating the outcome of RSV infection (19–22). IL-33 and TSLP were slightly increased with RSV infection, while MaR1 administration had no effect on their levels. IL-25 was also unperturbed with MaR1 administration (*SI Appendix*, Fig. S4). These data show a unique gene signature triggered by MaR1 in conjunction with increased interferon-β production, highlighting a type 1 interferon-dependent mechanism in reduction of viral transcripts.

Regulatory T Cells Express LGR6 and MaR1 Regulates Their Phenotype and Function During RSV Infection. Given the potent regulatory effect of MaR1 on virus-triggered type 2 inflammation, we profiled the expression of the recently discovered MaR1 receptor LGR6 (23) on inflammatory cell types by flow cytometry. Mouse macrophages expressed high levels of Lgr6 at baseline, which did not change significantly 6 d following RSV infection (*SI Appendix*, Fig. S5). B cells, ILCs (Lineage^{neg}), neutrophils, and eosinophils showed low levels of receptor expression at baseline and at day 6 pi (*SI Appendix*, Fig. S5). Mock-infected *FoxP3^{eGFP}* mice showed constitutive expression of Lgr6 on lung CD4$^+$ T cells, particularly Tregs (CD4$^+$FoxP3$^+$), and CD8$^+$ T cells expressed the receptor, but to a lower extent than Tregs (Fig. 4 *A*, *Left*). Of note, Lgr6 expression on Tregs was reduced on day 6 pi. Lgr6 expression increased back to near baseline levels on day 10 pi (Fig. 4 *A*, *Right*). To determine whether the change of Lgr6 expression on Tregs with RSV infection was associated with other phenotypic or functional changes, Tregs from mice on day 6 pi were probed for the type 2 master regulator, GATA-3, along with FoxP3 (i.e., type 2 Tregs) by flow cytometry. RSV infection led to higher numbers of GATA-3$^+$ CD4 TH2 cells (Fig. 4*B*). Type 2 Tregs expressing the dual transcription factors FoxP3, and GATA-3 were increased on day 6 pi and MaR1 significantly reduced the numbers of these pathologic RSV Tregs (Fig. 4*B*). A similar trend was seen by analyzing IL-13 cytokine production by flow cytometry (Fig. 4*C*). MaR1 significantly reduced the numbers of pathologic RSV Tregs expressing both FoxP3 and IL-13.

Pulmonary Tregs serve a critical role in restricting type 2 inflammation (24). Because Tregs express Lgr6 (Fig. 4*A*), we next determined whether MaR1 had direct actions on Tregs. Lung Tregs were isolated from mock- and RSV-infected *FoxP3^{eGFP}* mice that were exposed in vivo to MaR1 or a vehicle control (Fig. 4*D*). The ability of the isolated Tregs to suppress IL-13 production from ILC2 (IL-13$^+$Lineage$^-$) was determined using our recently developed assay of cell–cell interactions (15). ILCs were isolated from mice on day 6 pi with RSV and added to Tregs (ratio of 1:10; Treg/ILC). Supernatants from Treg/ILC co-cultures were harvested 72 h later and IL-13 levels were measured by ELISA. Tregs isolated from mock-infected mouse lungs inhibited IL-13 production by ILCs (Fig. 4*E*). Tregs from RSV-infected lungs were defective in their suppressive actions, failing to substantially inhibit IL-13 production by the ILCs (Fig. 4*E*). In contrast, Tregs from RSV-infected mice exposed to MaR1 showed significantly improved suppressive function, inhibiting IL-13 by approximately 40% (Fig. 4*D*). Treg-mediated suppression was dependent on transforming growth factor - β (TGF-β) signaling since a Smad3 inhibitor (SIS3) prevented their inhibition of IL-13 production, with IL-13 levels even higher than Tregs without SIS3 (Fig. 4*E*).

To translate these mechanistic insights from MaR1's actions on mouse Tregs, we next ascertained whether human Tregs expressed LGR6 and whether RSV infection had an impact on receptor expression. PBMCs from healthy donors were isolated and infected ex vivo with RSV (Multiplicity of infection (MOI) = 0.1), and 48 h pi, the cells were harvested and analyzed for LGR6 expression by flow cytometry. Human Tregs (CD3$^+$CD4$^+$CD45RA$^-$CD25$^+$CD127^{low}FoxP3$^+$) showed constitutive expression of LGR6, and its mean fluorescent Intensity (MFI) was significantly downregulated by RSV infection (Fig. 4*F*). These data demonstrate the translational potential for MaR1 regulation of Treg suppressive function and phenotype after RSV infection.

Lgr6-Deficient Mice Have Exacerbated Type 2 Immune Responses and Higher Viral Load. To assess the impact of MaR1–LGR6 signaling on inflammatory responses to RSV infection, we used Lgr6 knockout mice. *Lgr6$^{+/+}$* and *Lgr6$^{-/-}$* mice were infected with *RSV Line 19* (10^5 PFU, i.n.), and at day 6 pi, several parameters of pulmonary inflammation and viral burden were analyzed. *Lgr6$^{-/-}$* mice showed more mucous cell metaplasia as seen by PAS staining of lung sections compared to *Lgr6$^{+/+}$* mice (Fig. 5*A*). *gob5* transcripts levels and IL-13 protein levels in lung tissue were higher in *Lgr6$^{-/-}$* mice compared to *Lgr6$^{+/+}$* mice (Fig. 5 *B* and *C*). To determine whether Lgr6 was necessary for MaR1-mediated protective actions, cells were isolated from *Lgr6$^{+/+}$* and *Lgr6$^{-/-}$* lungs at day 6 pi and exposed to MaR1 (10ng/mL) ex vivo. Forty-eight hours post-MaR1 exposure, the cells were stimulated with phorbol ester, phorbol-12-myristate-13-acetate (PMA)/ionomycin in the presence of protein transport inhibitors and assessed by flow cytometry. Lungs from *Lgr6$^{-/-}$* mice had higher IL-13-expressing CD4 T cells and ILC cells compared to lungs from *Lgr6$^{+/+}$* mice (Fig. 5*D*). MaR1 exposure reduced the number of IL-13-expressing CD4 T cells and ILC cells in *Lgr6$^{+/+}$* lungs; however, this reduction was lost in *Lgr6$^{-/-}$* lungs (Fig. 5*D*).

Because MaR1 decreased the RSV-induced conversion of Tregs into GATA-3$^+$-expressing cells (Fig. 4*B*), we next evaluated lung Tregs day 6 pi in *Lgr6$^{+/+}$* and *Lgr6$^{-/-}$* mice. Flow cytometric analysis showed *Lgr6$^{-/-}$* mice had higher numbers of pathologic type 2 Tregs co-expressing FoxP3$^+$ and GATA-3$^+$ in the lungs compared to *Lgr6$^{+/+}$* mice (Fig. 5*E*). The increased type 2 expression profile was consistent with the increased *L* gene transcript seen in the *Lgr6$^{-/-}$* mice, indicating reduced ability to restrain RSV viral replication (Fig. 5*F*). Given the increase in pathologic type 2 Tregs in *Lgr6$^{-/-}$* mice after RSV infection, we next determined the capacity for MaR1–LGR6 interactions to augment de novo generation of Tregs. Naive T cells were polarized in vitro with TGF-β and MaR1 (see *Materials and Methods*). TGF-β alone robustly promoted the generation of Tregs from naïve CD4 T cells in the *Lgr6$^{+/+}$* and *Lgr6$^{-/-}$* mice (Fig. 5*G*). Co-incubation with TGF-β and MaR1 led to additive increases in FoxP3-expressing Tregs in the WT mice, but not in *Lgr6$^{-/-}$* mice (Fig. 5*G*). Of interest, AREG levels in the supernatants of these cell incubations were synergistically increased with dual administration of TGF-β and MaR1 in *Lgr6$^{+/+}$* mice, while this enhancing effect for Mar1 was lost in *Lgr6$^{-/-}$* mice, with AREG barely detectable (Fig. 5*H*). Taken together, this data indicates a critical role for MaR1 signaling via LGR6 on Treg number and functional suppression of type 2 immune responses after RSV infection.

MaR1 Regulates RSV-Induced Inflammatory Responses in Human Precision-Cut Lung Slices. To investigate whether the lung tissue mechanisms uncovered in mouse RSV infection translate to humans, we exposed human precision-cut lung slices (hPCLSs) from cryopreserved lungs of infants to *RSV line 19*. These hPCLSs retain airway epithelial function and have viable immune cell populations (25). The hPCLS were exposed to MaR1 (10 ng/mL) or vehicle and 6 h later were infected with *RSV line 19* (MOI 0.5). RSV infection induced significant cellular changes to

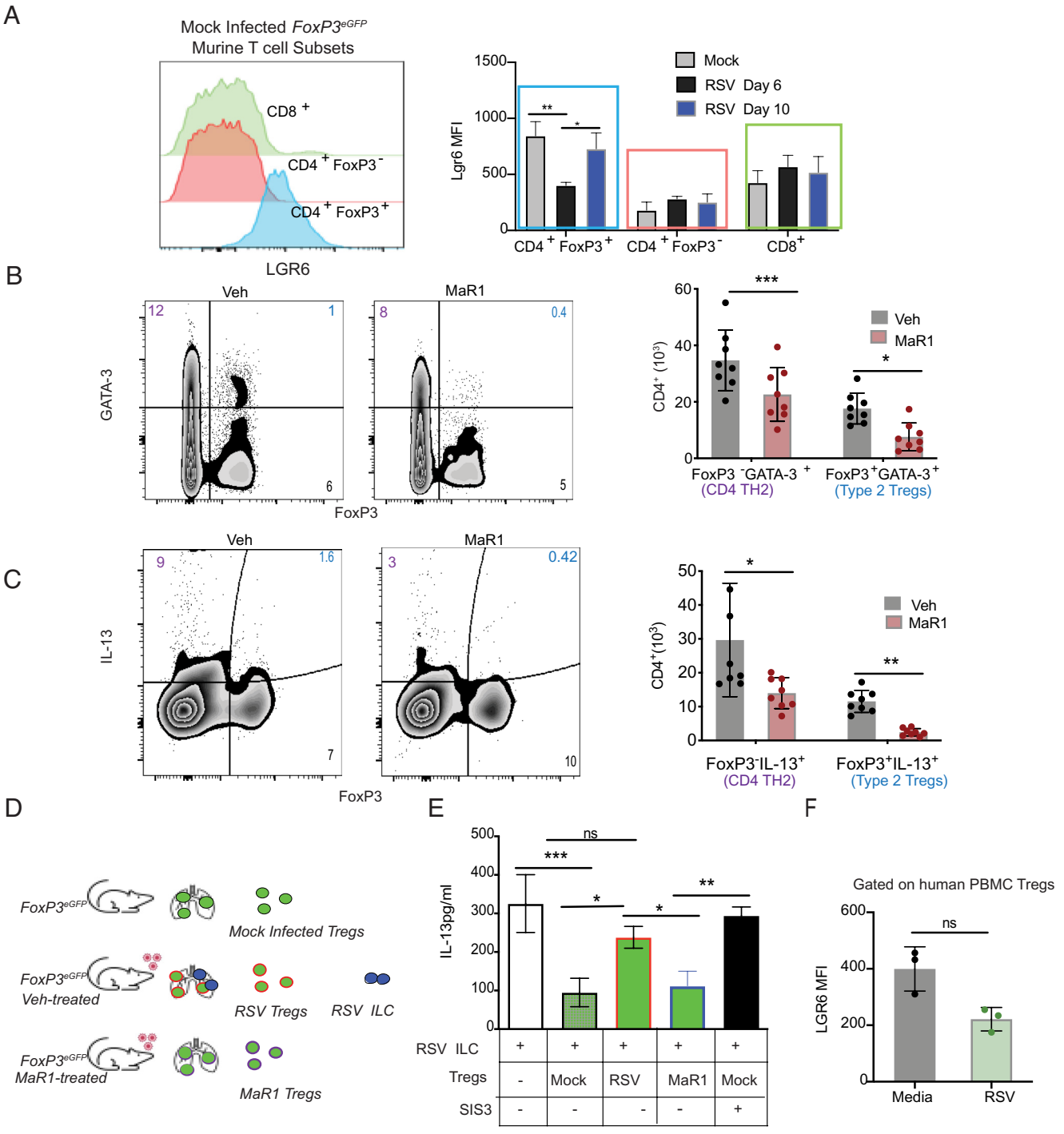

Fig. 4. Regulatory T cells express LGR6 and MaR1 regulates their phenotype and function during RSV infection. (*A*) Lgr6 expression on T cell subsets from mock infected *FoxP3*^{eGFP} mice. The *Left* panel shows the histogram, and the *Right* panel compares MFI of Lrg6 expression following Mock or RSV infection days 6 and 10 pi. (*B*) The expression of FoxP3 and GATA-3 within the CD4 population in lungs of RSV infected mice with or without MaR1 at day 6 pi as analyzed by flow cytometry and the quantification of cells. Values represent the mean ± SD. The data was analyzed using two-way ANOVA with Sidak's multiple comparisons test. *$P < 0.05$, ***$P < 0.001$. (*C*) The expression of FoxP3 and IL-13 within the CD4 population in lungs of RSV infected mice with or without MaR1 at day 6 pi as analyzed by flow cytometry and the quantification of cells. Values represent the mean ± SD. The data was analyzed using two-way ANOVA with Sidak's multiple comparisons test. *$P < 0.05$. (*D*) ILC2-Treg suppression was set from the different *FoxP3*^{eGFP} mice cohorts. ILC population were sorted from RSV-infected lungs day 6 pi and Tregs from mock and RSV-infected lungs day 6 pi ± MaR1 exposure were added to ILC2 (1:10 ratio). (*E*) IL-13 production was measured by ELISA 72 h after co-culture. Values represent the mean ± SD and the data was analyzed using one-way ANOVA with Tukey's multiple comparisons test. *$P < 0.05$, **$P < 0.01$, ***$P < 0.001$. The mouse experiments were performed twice and the data from the two experiments pooled. Each experiment used 3 to 4 mice per group. (*F*) Tregs were profiled from three healthy donors and the expression of LGR6 was analyzed by flow cytometry and expressed as MFI. The data was analyzed using Student's *t* test and NS.

the lung tissue 72 h pi as shown by phase-contrast microscopic images. These RSV-induced changes were substantially decreased with MaR1 pre-exposure (Fig. 6*A*). Similar to MaR1 counter-regulating mouse airway immune responses, MaR1 significantly decreased the RSV-triggered increases in IL-13 levels (Fig. 6*B*) and significantly increased AREG levels after RSV infection (Fig. 6*B*). We confirmed that the inhibition was not mediated by a decrease in IL-25, IL-33, or TSLP (*SI Appendix*, Fig. S6). Given the anti-viral role of MaR1 in promoting interferon-β in mouse lung tissues, the supernatant samples were analyzed for cytokine

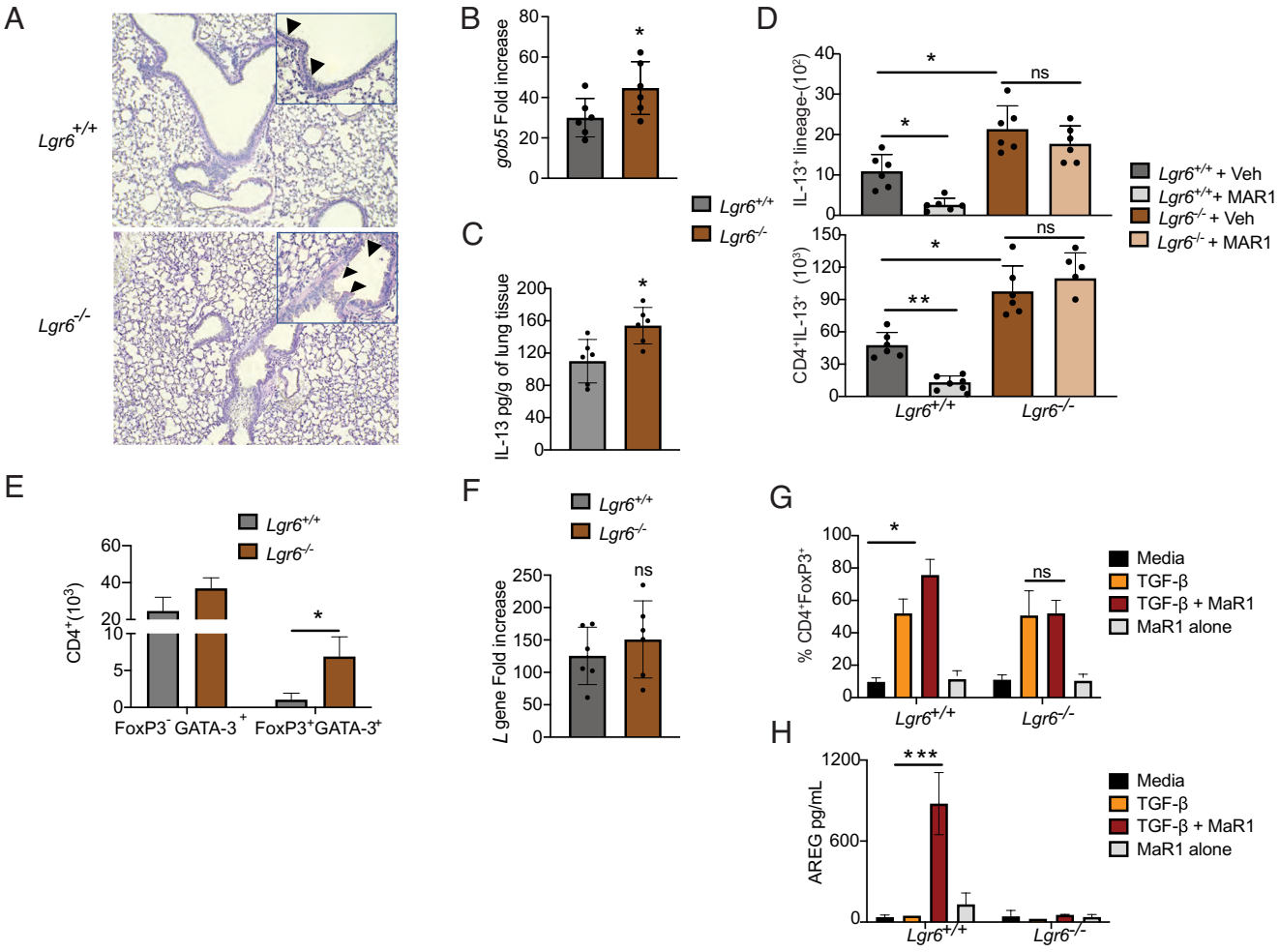

Fig. 5. Lgr6 deficient mice have exacerbated type 2 immune responses and higher viral load. 3-wk-old *Lgr6*$^{+/+}$ and *Lgr6*$^{-/-}$ mice were infected with *RSV line 19* and euthanized on day 6 pi. (*A*) PAS staining of lung sections. (*B*) *gob5* expression analysis by qRT-PCR. Fold increase was calculated over naïve *Lgr6*$^{+/+}$ and *Lgr6*$^{-/-}$ mice. Values represent the mean ± SD. *$P < 0.05$ using Student's *t* test. (*C*) IL-13 levels in lung tissue of *Lgr6*$^{+/+}$ and *Lgr6*$^{-/-}$ measured by ELISA. Values represent the mean ± SD. *$P < 0.05$ using Student's *t* test. (*D*) Number of IL-13^{+} Lineage^{-} ILC2 and IL-13^{+} CD4^{+} TH2 cells in the lungs of *Lgr6*$^{+/+}$ and *Lgr6*$^{-/-}$ mice with or without MaR1 ex vivo exposure as measured by flow cytometry. One-way ANOVA with Tukey's multiple comparisons test was performed. Values represent the mean ± SD. *$P < 0.05$, **$P < 0.01$. (*E*) Number of CD4 TH2 cells (FoxP3^{-} GATA-3^{+}) and type 2 Tregs (FoxP3^{+} GATA-3^{+}) in *Lgr6*$^{+/+}$ and *Lgr6*$^{-/-}$ mice as measured by flow cytometry. Error bars indicate mean ± SD. The data were analyzed by two-way ANOVA with Sidak's multiple comparison test. *$P < 0.05$. (*F*) RSV *L* gene expression analysis by qRT-PCR. Fold increase was calculated over naïve *Lgr6*$^{+/+}$ and *Lgr6*$^{-/-}$ mice. The data was analyzed using Student's *t* test and was NS. (*G*) In vitro generation of Tregs from naïve CD4 T cells isolated from spleens of *Lgr6*$^{+/+}$ and *Lgr6*$^{-/-}$ mice. The cells were analyzed for FoxP3 induction by flow cytometry after 4 d in culture with the addition of TGF-β, MaR1, or in combination. (*H*) The production of AREG from cell culture supernatants from *Lgr6*$^{+/+}$ and *Lgr6*$^{-/-}$ mice was measured by ELISA after the addition of TGF-β, MaR1, or in combination. This experiment was performed twice. Error bar indicate mean ± SD. The data for panels *G* and *H* were analyzed by two-way ANOVA with Sidak's multiple comparison test. *$P < 0.05$, ***$P<0.001$.

levels and MaR1 showed a trend towards increased production of interferon-β (Fig. 6*C*).

Discussion

The immunopathogenesis of RSV can produce substantial morbidity and mortality in vulnerable populations (1). Here, lung immune responses and their resolution after infection with a clinical strain of RSV were mapped out. *RSV line 19* evoked type 2 innate and adaptive immune responses that were associated with viral evasion of host control mechanisms and structural changes to the airways in infected mice. The virus crippled the immune-suppressive function of Tregs, converting them to prophlogistic effector cells. In this study, we have identified a pro-resolving signaling pathway with potent regulatory actions on RSV-induced airway inflammation involving the DHA-derived SPM MaR1 and its recently identified receptor LGR6 in orchestrating resolution of inflammation by controlling type 2 immune responses, countering RSV's subversion of Treg cell function, and increasing production of AREG. Together, these actions promoted lung catabasis, including enhanced viral clearance in a mouse model of RSV infection.

IL-13 is a potent inducer of mucin genes (16). At day 6 pi, the lung levels of this cytokine significantly increased and mucous cell metaplasia was present. IL-13 levels and *gob5* transcript expression in the mouse lung mirrored the viral burden as monitored by RSV *L* gene expression. The deficiency in IL-13 reduces mucous cell metaplasia following RSV infection and decreases viral burden (13, 16). Human volunteers infected with RSV display viral loads that correlate with mucus levels in nasal aspirates (26). Because IL-13 is a pivotal cytokine for airway type 2 immune responses and mucous cell metaplasia and exhibits a strong correlation to viral burden, we focused on RSV-induced IL-13. RSV triggered IL-13 production by both innate (ILCs) and adaptive (CD4 TH2 cells) lymphocytes. Six days pi, MaR1 reduced IL-13 production from these two cell types and reduced mucous cell metaplasia as evident from reduced *gob5* gene transcript levels. It is important to note that MaR1-mediated effects in reducing type 2 response were not mediated by targeting alarmin IL-33, TSLP, or IL-25.

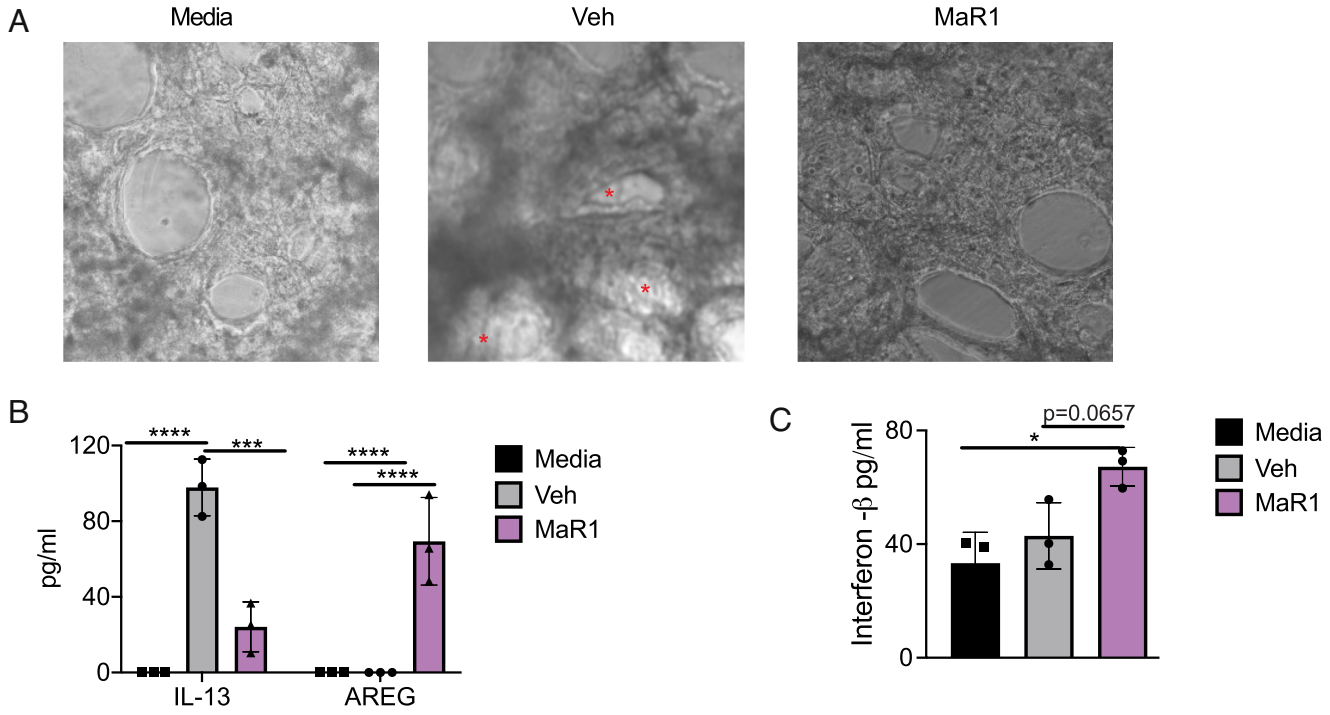

Fig. 6. MaR1 regulates RSV-induced inflammatory responses in hPCLSs. Human pediatric lung slices were infected with RSV ± MaR1. MaR1 was added to lung slices 24 h prior to infection. Seventy-two hours after the treatment, the following analyses were performed: (*A*) Phase contrast microscopy (airways indicated by red asterisk). (*B*) IL-13 and AREG protein levels in cell culture supernatant were measured by ELISA. The data were analyzed by two-way ANOVA with Sidak's multiple comparison test. ***P<0.001, ****P<0.0001. (*C*) Interferon-β in cell culture supernatant were measured by legend plex ELISA. This experiment was performed using three pediatric donors. The data were analyzed by one-way ANOVA with Tukey's multiple comparison test. *P<0.05.

The reduction in IL-13 levels with MaR1 was accompanied by decreased RSV L gene expression, suggesting that MaR1 disrupted the pathologic environment that had been conducive to viral replication after infection. The ability of MaR1 to upregulate gene transcripts of several pathways associated with anti-viral responses highlights the potency of SPMs in this viral model. There is also specificity of anti-viral action exhibited by SPMs with Protectin D1 promoting interferon-λ production in mouse lung tissues and primary human epithelial cells (27). These host protective actions for MaR1 may have clinical implications given that current anti-inflammatory treatments for RSV, including steroid administration, are associated with immunosuppression and increased susceptibility to other infections (1, 2).

Epithelial cell restitution is an important aspect of the resolution of airway inflammation, and AREG, an epithelial cell mitogen, aids in this process (28). The receptor for AREG is the epidermal growth factor receptor (EGFR). The fusion protein of *RSV line 19* interacts with EGFR to activate prophlogistic signaling (29). Sustained EGFR signaling potentiates the survival of RSV-infected epithelial cells, and thus an alternate ligand such as AREG could potentially decrease RSV pathogenesis (29, 30) and restore immune homeostasis. MaR1-mediated reduction in viral burden also correlated with increased AREG and decreased airway epithelial mucous cell metaplasia. In addition to the MaR1-induced AREG production by Tregs shown here, direct targeting of airway epithelium by the related DHA-derived SPMs protectin D1 and protectin conjugate of tissue regeneration 1 increased interferon-λ production to enhance viral host defense and promote the resolution of mouse RSV infection (31), suggesting that DHA metabolism to SPMs in response to viral respiratory tract infection leads to cell-type-specific responses that can work together to promote resolution of the pathogen-evoked airway inflammation. Of interest, compared to placebo control, omega-3 fatty acid supplementation of pregnant mothers with low endogenous DHA levels significantly reduces the risk for persistent wheeze and respiratory viral infections in their infants (12). There is evidence to suggest that SPM production might also be decreased in aging muscles of mice indicating that neonates and elderly might not have sufficient levels of SPMs for protection against viral infection (32). Our findings here suggest that DHA-derived SPMs could be important in protection against viral infections.

Immune responses to RSV are critical to promoting viral clearance, yet the type 2 immune responses in RSV drive pathology rather than protection (33). Tregs can exert their suppressive effect by curtailing pathologic cytokine production from ILC2 and CD4 TH2 cells, the major drivers of type 2 immunopathology in RSV infection (20, 34); however, pathologic responses to RSV are surprisingly exacerbated by Tregs after an RSV-induced switch in Tregs to an IL-13 producing prophlogistic cell phenotype (8). It is notable that MaR1 restored the suppressive function of the RSV type 2 Tregs as it reduced pathogen-elicited lung inflammation and mucous cell metaplasia. The MaR1 receptor LGR6 (23) was constitutively expressed at a high level on Tregs and macrophages with Treg LGR6 expression markedly changing during RSV infection. Macrophages are a critical source for MaR1 (14), and the sustained expression of LGR6 on macrophages enables autacoid regulation of macrophage responses for resolution (23). Lgr6-deficient mice were more susceptible to RSV-induced inflammation and had decreased Treg responses ex vivo to MaR1, highlighting the potent roles for MaR1 signaling and its receptor in host defense against RSV infections. In addition to important pro-resolving actions for MaR1–LGR6 signaling on macrophages, the increased pathologic type 2 Tregs in RSV-infected *Lgr6*$^{-/-}$ mice was consistent with Treg targeting by MaR1 in this experimental model.

SPMs are present in human maternal milk, suggesting roles for SPMs in priming the immature neonate immune system (35). Neonates, specifically preterm infants, are at risk for an omega-3 fatty acid deficit, and severe RSV infection (36). In addition to our findings here with mice, human Tregs also constitutively expressed LGR6. Exposing human pediatric lung slices to RSV infection decreased LGR6 expression on Treg. MaR1 also limited IL-13 levels and pathologic tissue responses when the human lung tissues were infected with RSV, consistent with translationally relevant protective actions for MaR1–LGR6 signaling in human tissues.

In summary, MaR1–LGR6 signaling regulated pathologic type 2 immune responses to RSV infection in mouse and human lungs. IL-13-producing innate and adaptive lymphocytes were integral to RSV pathogenesis, in part, because Treg-mediated control was disabled with RSV pathologic Tregs converted into prophlogistic effector lymphocytes. Tregs expressed LGR6 that could be targeted by the SPM MaR1, which restored Treg suppressive function, decreasing IL-13 and increasing AREG production in conjunction with accelerated viral clearance. Together, these findings point to a new pro-resolving function for SPMs in licensing Treg suppressive function that in RSV infection was amplified by MaR1–LGR6 signaling, suggesting a putative therapeutic target that is distinct from the current clinical approach emphasizing broad immunosuppression with corticosteroids.

Materials and Methods

Animals. *Balb/cByJ* (Stock Number: 001026) and *FoxP3*^{eGFP} (Stock Number: 006769) mice were purchased from The Jackson Laboratory. Mice were used at 3 w of age. Breeding pair of Lgr6-deficient mice (*Lgr6*$^{-/-}$) were obtained from Lehoczky and were originally from The Jackson Laboratory (Stock number 016934). All animal experiments were approved by the Institutional Animal Care and Use Committee (IACUC) at the Brigham and Women's Hospital. The protocol was approved by Harvard Medical Area (protocol number: 05115) and Brigham and Women's Hospital (protocol number: 2016N000357).

Virus Propagation, Quantification, and Mouse Model of Infection. *RSV line 19* is a clinical strain isolated originally from a sick infant in University of Michigan Health System that mimics human infection (37). The virus was propagated as previously described (31). Virus was propagated using Hep-2 cell line (American Tissue Culture Collection, ATCC) and quantified by visible plaque formation in STAT-1 deficient cell line (31). Mice were briefly anesthetized with isoflurane and infected intranasally with 1×10^5 pfu (plaque-forming units) of *RSV line 19*. MaR1 (10 ng/mouse) was administered via i.n. route on day 3 pi.

RSV Infection of hPCLSs. The hPCLS from young infants were generated as described in prior study (25). Lungs were purchased from International Institute for the Advancement of Medicine, a nonprofit institute that provides non-transplantable human tissues for medical research. These donor lungs were de-identified and were from children (0 to 5 y of age). The frozen lung slices were thawed at 37 °C and rested overnight in complete RPMI media. Two lung slices were plated per well in a 12-well plate with 1 mL of media. These slices were exposed to MaR1 (10 ng/mL; 6 h prior to infection) or vehicle and then infected with *RSV line 19* (MOI 0.5). Seventy-two hours after infection, the cell culture supernatants were harvested and analyzed by ELISA for cytokine production.

RSV Infection of Human Peripheral Blood Mononuclear Cells (PBMCs). Human PBMCs were isolated from de-identified blood donors, as previously described (38). The frozen PBMCs were thawed at 37 °C plated (1 million/mL) in complete RPMI media. One hour following the plating, the cells were infected with *RSV line 19* (MOI 0.1). Forty-eight hours after the infection, the cells were harvested and analyzed by flow cytometry.

Antibody and Flow Cytometry. The following antibodies were used in flow cytometry with the indicated antibody clones and manufacturers for the mouse experiments: Anti-CD3 (17A2; BD Biosciences), anti-CD19 (6D5; BioLegend), anti-CD11c (clone: N418; Biolegend), anti-CD11b (M1/70; BioLegend), anti-CD49b (DX5; eBioscience), anti-CD25 (PC61; BD Biosciences), anti-CD90.2 (anti-Thy-1.2; 53 2.1; eBioscience), anti-CD11c (N418; eBioscience), anti-ST2 (DIH9; BioLegend), anti-Siglec-F (clone: E50-2440; Biolegend) anti-CD4 (RM4-5; BD Biosciences), anti-IL-13 (ebio13A, eBioscience), anti-Foxp3 (FJK-16S; eBioscience), anti-CD62L(MEL-14; eBioscience), LGR6 (17658-1-AP; Proteintech). Flow cytometric data acquisition was performed on an LSRFortessa flow cytometer (BD Biosciences), and the data analyzed using FlowJo software version 10.3 (Tree Star). The gating strategy is provided in *SI Appendix*, Fig. S7 for populations analyzed.

Mouse Single Cell Lung Preparation. The lungs were perfused with sterile PBS, removed, and digested as described previously (8, 15). Lungs were then dissociated with a gentle MACS Dissociator (Miltenyi Biotech) according to the manufacturer's protocol. Single-cell suspensions were obtained by passing the dissociated tissue through a 70 μm cell strainer (BD Falcon).

ILC/Treg Co-culture. ILCs were isolated from RSV-infected mice and seeded at 50,000 cells/well in cRPMI. Tregs were isolated from *FoxP3*^{eGFP} and the ratio of ILC/Tregs was at 10:1. To activate ILC2 in the pool of ILC, IL-7 (10 ng/mL; Biolegend) was added. Tregs were activated with plate-bound anti-CD3 and soluble CD28 (2 μg/mL). Seventy-two hours post-stimulation, cell culture supernatants were collected and analyzed for IL-13 levels by ELISA.

Airway Inflammation. Lungs were perfused and fixed with zinc fixative (BD Pharmingen) at 20 cm H_2O, and histology performed as previously described (15). Tissues were embedded, sectioned, and stained with hematoxylin and eosin or PAS staining by the Dana Farber/Harvard Cancer, Center Rodent Histopathology Core, or the Brigham and Women's Pulmonary and Critical Care Medicine Histology Core. The samples for H&E shown in *SI Appendix*, Fig. S2 were scored in a blinded manner by author Dr. Cagnina who was not involved in the samples collection or processing or any other aspect of the experiment.

ELISA. Mouse IL-13, AREG, and human IL-25 ELISA kits were purchased from R&D Systems and used according to the manufacturer's instructions. Mouse legend plex was used for IL-33, IL-25, TSLP, and interferon-β were purchased from BioLegend.

RNA Isolation and Quantitative PCR. Messenger RNA (mRNA) was isolated using TRIzol as previously described (39), and complementary DNA (cDNA) was generated from DNase-treated mRNA using a reverse transcription kit (Life Technologies). Quantitative PCR was performed using EvaGreen master mix (BioRad) or TaqMan primers and universal master mix (Life Technologies) on the Mx3005P system (Agilent Technologies). The primers for *il13, gob5,* and RSV *Large polymerase (L)* gene (31) were purchased from IDT and relative gene expression was determined as $2^{-\Delta\Delta CT}$ (39).

PCR Array. The PCR array was performed according to the manufacturer's instructions. mRNA was isolated as stated above. cDNA was generated from DNase-treated mRNA using a reverse transcription kit (Life Technologies). The amplified cDNA was diluted with nuclease-free water 1.5 and added to the *RT*^{2} *qPCR* array (Qiagen, MD). The PCR array was for mouse anti-viral response. cDNA from each mouse per group per time point was coated on an individual plate. The genes were normalized to house-keeping gene β-actin.

Statistics. Student's unpaired two-tailed *t* test was used for all statistical analyses comparing two groups. For comparisons with more than two groups, one-way ANOVA with Tukey's for multiple comparisons test or two-way ANOVA with Sidak's multiple comparison test was used. All statistical analyses were performed with GraphPad Prism. Results are expressed as mean ± SD. Differences between the groups were considered significant if $P<0.05$.

$^*P<0.05$, $^{**}P<0.01$, $^{***}P<0.001$. All data are representative of at least two independent experiments with a minimum of three mice per group in each experiment.

Data, Materials, and Software Availability. No new transgenic mice or cell lines were developed in this part of study. The data are provided in the main text and *SI Appendix*. All other data are included in the article and/or *SI Appendix*.

ACKNOWLEDGMENTS. We thank Dr. Nicholas Lukacs (University of Michigan, Ann Arbor MI) for providing the RSV clinical isolate strain Line 19, and Dr. Joan Durbin (Rutgers, New Jersey Medical School) for providing the STAT1$^{-/-}$ cell line for RSV plaque assay. Funding:This work was supported by NIH P01GM095467, R01HL122531(to B.D.L.) and R56HL155917 (to N.K.). N.K. was also supported by a Fund to Sustain Research Excellence Award from BWH.

Author affiliations: [a]Pulmonary and Critical Care Medicine Division, Department of Medicine, Brigham and Women's Hospital, Harvard Medical School, Boston, MA 02115; [b]Neonatology Division, Mass General Hospital for Children, Boston, MA 02114; and [c]Department Of Orthopedic Surgery, Brigham and Women's Hospital, Harvard Medical School, Boston, MA 02115

Author contributions: N.K. and B.D.L. designed research; N.K., K.H.W., T.R.B., L.P.T., E.W.S., Y.B., X.A., R.E.C., M.G.D., and J.A.L. performed research; N.K., K.H.W., T.R.B., L.P.T., E.W.S., Y.B., X.A., R.E.C., M.G.D., J.A.L., and B.D.L. analyzed data; J.N. editing and submission; and N.K., J.N., and B.D.L. wrote the paper.

1. H. Nair *et al.*, Global burden of acute lower respiratory infections due to respiratory syncytial virus in young children: A systematic review and meta-analysis. *Lancet* **375**, 1545–1555 (2010).
2. K. M. Empey, R. S. Peebles Jr., J. K. Kolls, Pharmacologic advances in the treatment and prevention of respiratory syncytial virus. *Clin. Infect. Dis.* **50**, 1258–1267 (2010).
3. J. A. Coultas, R. Smyth, P. J. Openshaw, Respiratory syncytial virus (RSV): A scourge from infancy to old age. *Thorax* **74**, 986–993 (2019).
4. M. Ramaswamy, D. J. Groskreutz, D. C. Look, Recognizing the importance of respiratory syncytial virus in chronic obstructive pulmonary disease. *COPD* **6**, 64–75 (2009).
5. D. Linden *et al.*, Respiratory viral infection: A potential "missing link" in the pathogenesis of COPD. *Eur. Respir Rev.* **28**, 180063 (2019).
6. G. Piedimonte, M. K. Perez, Respiratory syncytial virus infection and bronchiolitis. *Pediatr Rev.* **35**, 519–530 (2014).
7. S. Z. Josefowicz, L. F. Lu, A. Y. Rudensky, Regulatory T cells: Mechanisms of differentiation and function. *Annu. Rev. Immunol.* **30**, 531–564 (2012).
8. N. Krishnamoorthy *et al.*, Early infection with respiratory syncytial virus impairs regulatory T cell function and increases susceptibility to allergic asthma. *Nat. Med.* **18**, 1525–1530 (2012).
9. N. Krishnamoorthy, R. E. Abdulnour, K. H. Walker, B. D. Engstrom, B. D. Levy, Specialized proresolving mediators in innate and adaptive immune responses in airway diseases. *Physiol. Rev.* **98**, 1335–1370 (2018).
10. M. C. Basil, B. D. Levy, Specialized pro-resolving mediators: Endogenous regulators of infection and inflammation. *Nat. Rev. Immunol.* **16**, 51–67 (2016).
11. C. N. Serhan, B. D. Levy, Resolvins in inflammation: Emergence of the pro-resolving superfamily of mediators. *J. Clin. Invest.* **128**, 2657–2669 (2018).
12. H. Bisgaard *et al.*, Fish oil-derived fatty acids in pregnancy and wheeze and asthma in offspring. *N Engl. J. Med.* **375**, 2530–2539 (2016).
13. N. W. Lukacs *et al.*, Differential immune responses and pulmonary pathophysiology are induced by two different strains of respiratory syncytial virus. *Am. J. Pathol.* **169**, 977–986 (2006).
14. C. N. Serhan *et al.*, Macrophage proresolving mediator maresin 1 stimulates tissue regeneration and controls pain. *FASEB J.* **26**, 1755–1765 (2012).
15. N. Krishnamoorthy *et al.*, Cutting edge: Maresin-1 engages regulatory T cells to limit type 2 innate lymphoid cell activation and promote resolution of lung inflammation. *J. Immunol.* **194**, 863–867 (2015).
16. S. Mukherjee, N. W. Lukacs, Association of IL-13 in respiratory syncytial virus-induced pulmonary disease: Still a promising target. *Expert Rev. Anti Infect. Ther.* **8**, 617–621 (2010).
17. M. S. Lo, R. M. Brazas, M. J. Holtzman, Respiratory syncytial virus nonstructural proteins NS1 and NS2 mediate inhibition of Stat2 expression and alpha/beta interferon responsiveness. *J. Virol.* **79**, 9315–9319 (2005).
18. H. Hammad, B. N. Lambrecht, Barrier epithelial cells and the control of type 2 immunity. *Immunity* **43**, 29–40 (2015).
19. L. Abramowitz *et al.*, Systematic evaluation and description of anal pathology in HIV-infected patients during the HAART era. *Dis. Colon Rectum* **52**, 1130–1136 (2009).
20. M. T. Stier *et al.*, Respiratory syncytial virus infection activates IL-13-producing group 2 innate lymphoid cells through thymic stromal lymphopoietin. *J. Allergy Clin. Immunol.* **138**, 814–824.e811 (2016).
21. C. A. Malinczak *et al.*, Sex-associated TSLP-induced immune alterations following early-life RSV infection leads to enhanced allergic disease. *Mucosal Immunol.* **12**, 969–979 (2019).
22. B. C. Petersen, V. Dolgachev, A. Rasky, N. W. Lukacs, IL-17E (IL-25) and IL-17RB promote respiratory syncytial virus-induced pulmonary disease. *J. Leukoc Biol.* **95**, 809–815 (2014).
23. N. Chiang, S. Libreros, P. C. Norris, X. de la Rosa, C. N. Serhan, Maresin 1 activates LGR6 receptor promoting phagocyte immunoresolvent functions. *J. Clin. Invest.* **129**, 5294–5311 (2019).
24. A. Ray, A. Khare, N. Krishnamoorthy, Z. Qi, P. Ray, Regulatory T cells in many flavors control asthma. *Mucosal Immunol.* **3**, 216–229 (2010).
25. Y. Bai *et al.*, Cryopreserved human precision-cut lung slices as a bioassay for live tissue banking. A viability study of bronchodilation with bitter-taste receptor agonists. *Am. J. Respir Cell Mol. Biol.* **54**, 656–663 (2016).
26. R. S. Thwaites *et al.*, Reduced nasal viral load and IFN responses in infants with respiratory syncytial virus bronchiolitis and respiratory failure. *Am. J. Respir Crit. Care Med.* **198**, 1074–1084 (2018).
27. K. H. Walker *et al.*, Protectins PCTR1 and PD1 reduce viral load and lung inflammation during respiratory syncytial virus infection in mice. *Front Immunol.* **12**, 704427 (2021).
28. A. M. Jamieson *et al.*, Role of tissue protection in lethal respiratory viral-bacterial coinfection. *Science* **340**, 1230–1234 (2013).
29. M. G. Currier *et al.*, EGFR interacts with the fusion protein of respiratory syncytial virus strain 2–20 and mediates infection and mucin expression. *PLoS Pathog.* **12**, e1005622 (2016).
30. M. M. Monick *et al.*, Activation of the epidermal growth factor receptor by respiratory syncytial virus results in increased inflammation and delayed apoptosis. *J. Biol. Chem.* **280**, 2147–2158 (2005).
31. K. H. Walker *et al.*, Protectins PCTR1 and PD1 reduce viral load and lung inflammation during respiratory syncytial virus infection in mice. *Front. Immunol.* **12**, 704427 (2021).
32. J. F. Markworth *et al.*, Metabolipidomic profiling reveals an age-related deficiency of skeletal muscle pro-resolving mediators that contributes to maladaptive tissue remodeling. *Aging Cell* **20**, e13393 (2021).
33. J. E. Johnson, R. A. Gonzales, S. J. Olson, P. F. Wright, B. S. Graham, The histopathology of fatal untreated human respiratory syncytial virus infection. *Mod. Pathol.* **20**, 108–119 (2007).
34. J. Saravia *et al.*, Respiratory syncytial virus disease is mediated by age-variable IL-33. *PLoS Pathog.* **11**, e1005217 (2015).
35. H. Arnardottir, S. K. Orr, J. Dalli, C. N. Serhan, Human milk proresolving mediators stimulate resolution of acute inflammation. *Mucosal Immunol.* **9**, 757–766 (2016).
36. K. D. Lewis, J. Conway, C. Cunningham, B. M. K. Larsen, Optimizing nutrition in pediatric heart failure: The crisis is over and now it's time to feed. *Nutr. Clin. Pract* **33**, 397–403 (2018).
37. M. L. Herlocher *et al.*, Immunological properties of plaque purified strains of live attenuated respiratory syncytial virus (RSV) for human vaccine. *Vaccine* **17**, 172–181 (1999).
38. M. G. Duvall *et al.*, Human NK cell cytoskeletal dynamics and cytotoxicity are regulated by LIM kinase. *J. Immunol.* **205**, 801–810 (2020).
39. J. K. Colby *et al.*, Resolvin D3 and aspirin-triggered resolvin D3 are protective for injured Epithelia. *Am. J. Pathol.* **186**, 1801–1813 (2016).